Bioelectrochemistry 145 (2022) 108085

Contents lists available at ScienceDirect

Bioelectrochemistry

journal homepage: www.journals.elsevier.com/bioelectrochemistry

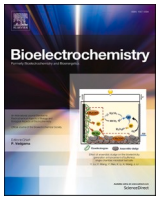

Cascade i-motifs-dependent reversible electrochemical impedance strategy-oriented pH and terminal deoxynucleotidyl transferase biosensing

Yudi Zheng [a,1], Dandan Hu [a,1], Di Wu [c,1], Kaiyue Hu [a], Xinxin Ren [a], Lingxia Qin [a], Zhiyong Guo [a], Sui Wang [a], Yufang Hu [a,b,*], Shaohua Ma [c,*]

[a] State Key Laboratory for Managing Biotic and Chemical Threats to the Quality and Safety of Agro-products, State Key Laboratory Base of Novel Functional Materials and Preparation Science, School of Materials Science & Chemical Engineering, Ningbo University, Ningbo, Zhejiang 315211, China
[b] State Key Laboratory of Chemo/Biosensing and Chemometrics, College of Chemistry and Chemical Engineering, Hunan University, Changsha, Hunan 410082, China
[c] College of Medical Technology, Ningbo College of Health Sciences, Ningbo 315100, China

ARTICLE INFO

Keywords:
Terminal deoxynucleotidyl transferase
pH
Electrochemical impedance spectroscopy
Cascade i-motifs
Biosensing

ABSTRACT

In this study, we develop a novel and reversible electrochemical impedance strategy for pH and terminal deoxynucleotide transferase (TdT) analysis based on the TdT-assisted generation of long enough cytosine (C)-rich DNAs. The formation of this special DNA is rationally designed on 5′-thiol DNA modified Au electrode surface, and TdT can catalyze the extension of this 3′-OH end to form a long C-rich DNA in the presence of deoxycytidine triphosphate (dCTP). Here, we discover a reversible process, in which the TdT-generated C-rich DNA maintains an irregular single chain state under neutral conditions and some stable DNA i-motifs (cascade i-motifs) are formed due to the partial protonation of C under acidic conditions. More importantly, the electrochemical impedance spectroscopy (EIS) response varies with the configuration change of the TdT-mediated C-rich DNA under different pH conditions. In view of this, a unique EIS switch ("on-off-on") is constructed faithfully with the configuration change, thus achieving pH analysis well. Additionally, the TdT activity can be also detected well by recording the EIS response, because it can catalyze the DNA tailing process up to hundreds of cytosines; on the contrary, if its inhibitor exists, TdT-based extension and formation of cascade i-motifs will not occur. Using this strategy, the detection of limit for TdT is 0.79×10^{-5} U/mL (pH 7.0) and 0.25×10^{-5} U/mL (pH 5.8) (S/N = 3), respectively. All the above features make our biosensor a promising assay for *in situ* monitoring of pH and TdT in complex clinical diagnosis.

1. Introduction

Typically, four-stranded DNA secondary structures can be formed by rich cytosine (C-rich) sequences under certain conditions, which is called the intercalated motif (i-motif) structure [1,2]. In general, this i-motif is composed of two parallel-stranded DNA duplexes, which are assembled together in an antiparallel orientation by intercalated and protonated cytosine pairs ($C{\cdot}C^{+}$) [3]. Previously, the first NMR tetramolecular i-motif, which involves the highly symmetric stranded association under acidic conditions, is reported in 1993 [4]. Since then many researchers extensively focus their attention on the study of these i-motif structures [5]. So far, the i-motif structures in the end of telomeres and the regions of oncogene promoters have been identified successfully [6,7], which can serve as the targets of drugs for cancer's treatment owing to their important biological functions. Some studies indicate that the i-motif conformations with $C{\cdot}C^{+}$ pairs are closely related to pH conditions, which are comparatively stable in weakly acidic conditions [8,9]. Therefore, the unique i-motif topology and property are also widely used in the different fields, such as DNA machines [10,11], logic operations [12,13], and pH monitoring [8,14]. However, as we have seen, these i-motif-based cases have mostly focused on the understandings of single i-motif DNA and its structural details, more importantly, cascade i-motifs have not been reported so far, also a challenging task.

* Corresponding authors at: State Key Laboratory for Managing Biotic and Chemical Threats to the Quality and Safety of Agro-products, State Key Laboratory Base of Novel Functional Materials and Preparation Science, School of Materials Science & Chemical Engineering, Ningbo University, Ningbo, Zhejiang 315211, China (Y. Hu).
E-mail addresses: huyufang@nbu.edu.cn (Y. Hu), 396919913@qq.com (S. Ma).
[1] These authors contributed equally to this work.

https://doi.org/10.1016/j.bioelechem.2022.108085
Received 7 December 2021; Received in revised form 29 January 2022; Accepted 7 February 2022
Available online 17 February 2022

To our knowledge, abnormal fluctuations in pH (a significant parameter for human health) not only can serve as an indicator for dehydration, metabolic activity, and so on, but also can lead to several diseases involving stroke, cancer, and so forth [15,16]. Therefore, monitoring the change in pH plays a vital role in understanding the pathology and physiology of organisms. So far, several techniques for detecting pH have been employed extensively including electrochemistry [17,18], fluorescence [19,20] and surface-enhanced Raman scattering [21,22]. Among the mentioned cases above, electrochemical sensor can be made by using cheap materials and be miniaturized easily into portable devices, which is strong candidates for fulfilling the requirements of ubiquitous sensing [23,24]. Integrating cascade DNA i-motifs with electrochemical technique provides a good idea for pH monitoring, which has not been reported yet.

Based on our knowledge, biological enzyme-induced catalytical processes play important role in cell proliferation, senescence, and gene transcription [25,26]. Herein, a calf thymus DNA polymerase, called terminal deoxynucleotidyl transferase (TdT), stood out because of template-free catalytic polymerization function [27]. In fact, TdT, which mainly distributes in the thymus and bone marrow of human tissue, can catalyze the polymerization of deoxynucleotides to the 3′-OH end of DNA molecules [28]. A growing body of researches show that TdT can act as a biomarker for some cancers, especially routine diagnosis of acute leukemia, which has greatly crucial physiological and biological significance [29,30]. The traditional analytical methods involve mainly gel electrophoresis and immunoassay, which suffer from complicated operation, radioactive contamination, and sophisticated procedures. Recently, other methods including colorimetric, electrochemical, fluorescent and chemiluminescent analysis have been developed successively [31-33]. However, it is worth mentioning that acid-base dysregulation in human body is a universal phenomenon of cancer cells, and of course TdT-related diseases are also included, which will have a great impact on the uptake and efficacy of pH-sensitive chemotherapeutic drugs. Fortunately, the pH-sensitive reversible biosensor can accommodate timely this change and alarm proactively to enhance reliability of the system in complex matrix. From this perspective, it is highly desirable to exploit an efficient, sensitive and convenient strategy to *in situ* probe TdT activity in complex and fluctuant pH matrix.

Inspired by that, an economic and facile electrochemical impedance strategy is developed based on pH-sensitive reversible cascade i-motifs to achieve the monitoring of pH in sweat samples and the detection of TdT in cell lysate samples. In this work, deoxycytidine triphosphate (dCTP) can be added continuously to the 3′-OH end of single-stranded DNA to form a long C-rich DNA [34-36], moreover, the C-rich DNA can be half-protonated to form i-motif structure via hydrogen bonding [3-8]. In view of the fact, for the first time, our proposed work is designed for an integral whole of the generation of long C-rich DNA, the formation of cascade DNA i-motifs, and the variation of electrochemical impedance spectroscopy (EIS). On the one hand, we construct a unique EIS switch ("on-off-on") via pH-derived configurational change of TdT-extended long C-rich DNA, thus achieving favourably pH analysis; on the other hand, the EIS signal is closely related to the activity of TdT, so a reversible EIS strategy is developed firstly for probing TdT activity and its inhibitors. In the process, the EIS response along with the formation of TdT-extended C-rich DNA under the neutral condition becomes larger; on the other hand, the EIS response after the construction of cascade i-motifs becomes smaller. Hence, the novel EIS biosensor can be further applied for TdT analysis in different pHs. All these, it lays a solid foundation to strive for new victories on *in situ* monitoring TdT activity sensitively in clinical bioanalysis in the future.

2. Experimental

2.1. Chemicals and materials

Terminal deoxynucleotidyl transferase (TdT), TdT buffer (1 M potassium cacodylate, 0.125 M Tris, 0.05% (v/v) Triton X-100, 5 mM $CoCl_2$ (pH 7.2)), deoxycytidine triphosphate (dCTP) and original DNAs (1, 5′- GTGAAT-3′, used in homogeneous system; 2, 5′-SH-GTGAAT-3′, employed in electrochemical system) were provided by Sangon Biotech. Co. Ltd (Shanghai, China). $Na_4P_2O_7{\cdot}10H_2O$ (PP) was purchased from Sinopharm Chemical Reagent Co. Ltd (Shanghai, China). Histone acetyltransferase (HAT), uracil-DNA glycosylase (UDG), protein kinase A (PKA), alkaline phosphatase (ALP), glucose oxidase (GOx), and 6-mercaptohexanol (MCH) were ordered from Sigma-Aldrich (Shanghai, China). All other chemicals were of analytical grade without further purification. Double-distilled water obtained from a Millipore Milli-Q system was used throughout.

2.2. Apparatus

A CHI 760E electrochemical workstation (Shanghai Chenhua Instruments Co., China) was used for accomplishing all electrochemical measurements, and a typical three-electrode system was employed: a gold working electrode (Au, 2 mm in diameter), a platinum wire counter electrode and a saturated Ag/AgCl reference electrode. Polyacrylamide gel electrophoresis (PAGE) was scanned by a ChemiDoc™ MP System (Bio-Rad). Dynamic light scattering (DLS) was performed from a Malvern Zana ZS 90 Mastersizer (UK). The extinction of AuNPs was tested from 400 to 800 nm by a TECAN microplate reader. Circular dichroism spectra (CD) were achieved by a JASCO J-815 spectropolarimeter (Tokyo, Japan).

2.3. Fabrication of the electrodes

Firstly, all bare Au electrodes were pretreated by a conventional process, which was presented in Supporting Information. Then, Au electrodes after treatment were immersed into the immobilization buffer containing the original DNA solution (0.5 μM) for overnight at 4 °C. After washing, the electrodes were put into MCH solution (1 mM) for 30 min to remove redundant sites. Next, a mixture of 0.5 μL dCTP (10 mM), 0.1 μL TdT (5 U/mL), TdT buffer (1 μL) and double-distilled water (0.9 μL) was coated onto the modified surface above for 180 min at 37 °C, then rinsed thoroughly with the cleaning buffer.

2.4. pH and TdT biosensing

The electrodes after TdT extension were immersed into PB (100 mM) with different pHs (4.0, 4.2, 4.5, 4.8, 5.0, 5.2, 5.4, 5.6, 5.8, 6.0, 6.2, 6.4, 6.6, 6.8, 7.0, 7.2, 7.5, 7.8, and 8.0) for 25 min at room temperature, and then transferred into the corresponding PB (100 mM) but containing 5 mM $[Fe(CN)_6]^{3-/4-}$ for the following electrochemical EIS measurements.

For TdT activity analysis: on the one hand, TdT at various final concentrations (0, 1×10^{-5}, 2×10^{-5}, 5×10^{-5}, 8×10^{-5}, 1×10^{-4}, 2×10^{-4}, 5×10^{-4}, 1×10^{-3}, 2×10^{-3}, 5×10^{-3}, 1×10^{-2}, 2×10^{-2}, 5×10^{-2}, 1×10^{-1}, 2×10^{-1}, and 5×10^{-1} U/mL) were employed for performing TdT-mediated extension process in Section 2.3 (other steps kept the same); on the other hand, PP (0.4 μL) at various final concentrations (0, 0.005, 0.01, 0.015, 0.02, 0.025, 0.03, 0.035, 0.04, 0.045, 0.05, and 0.06 mM) were introduced into TdT reaction solution above under other fixed conditions.

3. Results and discussion

Our investigation on cascade i-motifs-dependent reversible electrochemical impedance strategy-oriented pH and terminal deoxynucleotidyl transferase biosensing involves four main areas: the design and preparation of unique cascade i-motif probes, the study on i-motif configuration change accompanied by different pHs, the sensitive analysis for direct detection of human sweat collected from dehydrated skin, and the label-free and special test for TdT activity and its inhibitors.

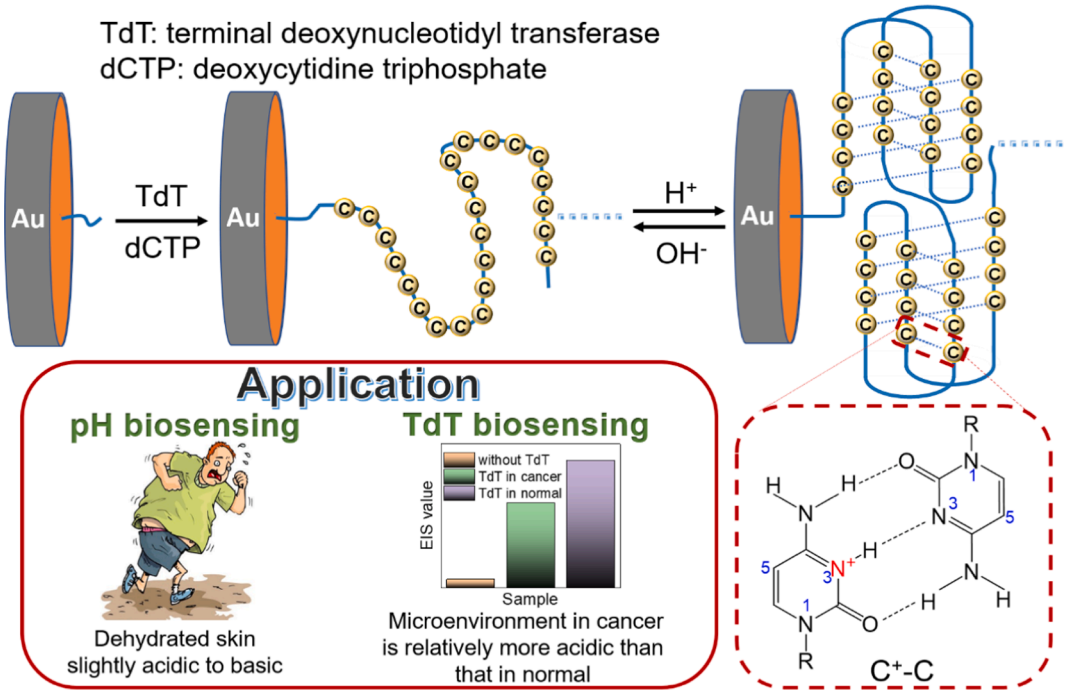

Scheme 1. Schematic illustration of cascade i-motifs-dependent electrochemical impedance strategy and its application on pH and terminal deoxynucleotidyl transferase (TdT) biosensing.

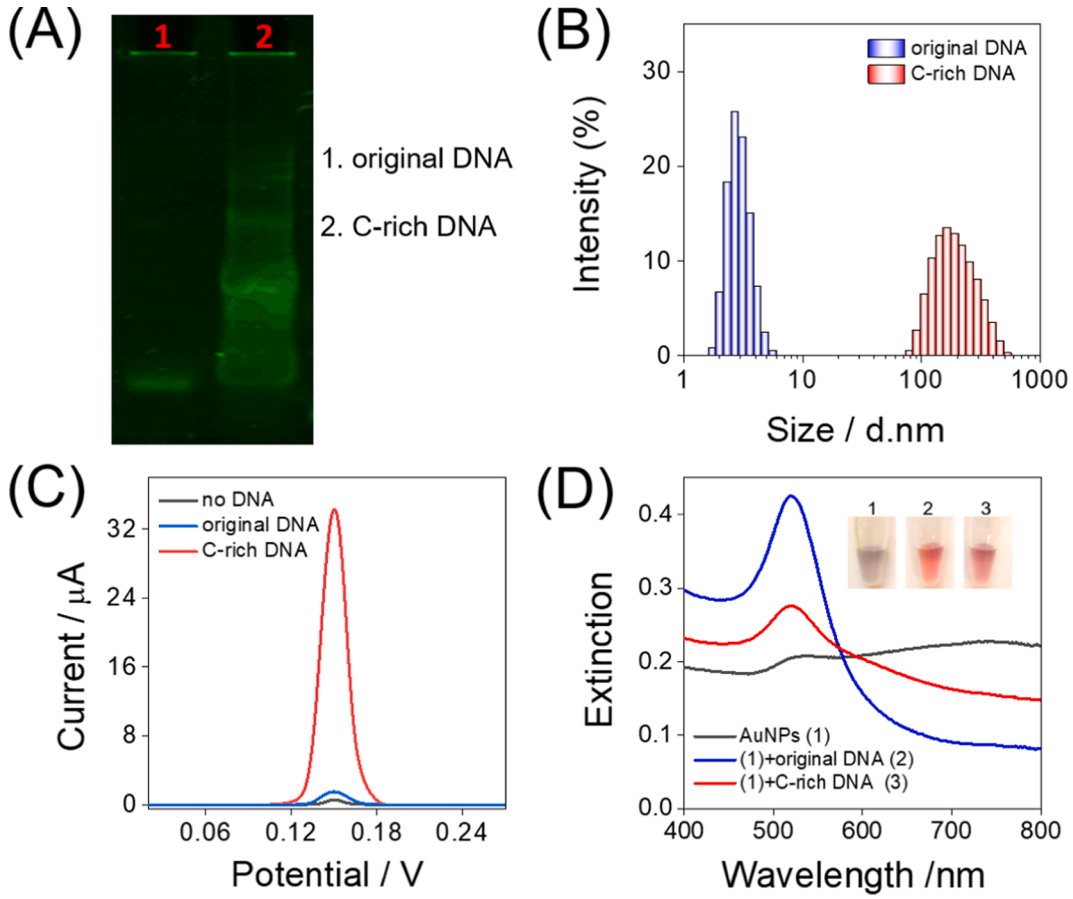

Fig. 1. Formation of TdT-yielded C-rich DNA: (A) PAGE image for characterizing TdT-yielded C-rich DNA; (B) Size distributions on original DNA and C-rich DNA determined by dynamic light scattering; (C) Square wave voltammetry (SWV) measurements on original DNA and C-rich DNA after the treatment of 100 μM Ag(I); (D) UV–vis spectra of 13 nm AuNPs (5 nM), original DNA and C-rich DNA adsorption on AuNPs in the presence of 50 mM NaCl, inset: the corresponding photographs.

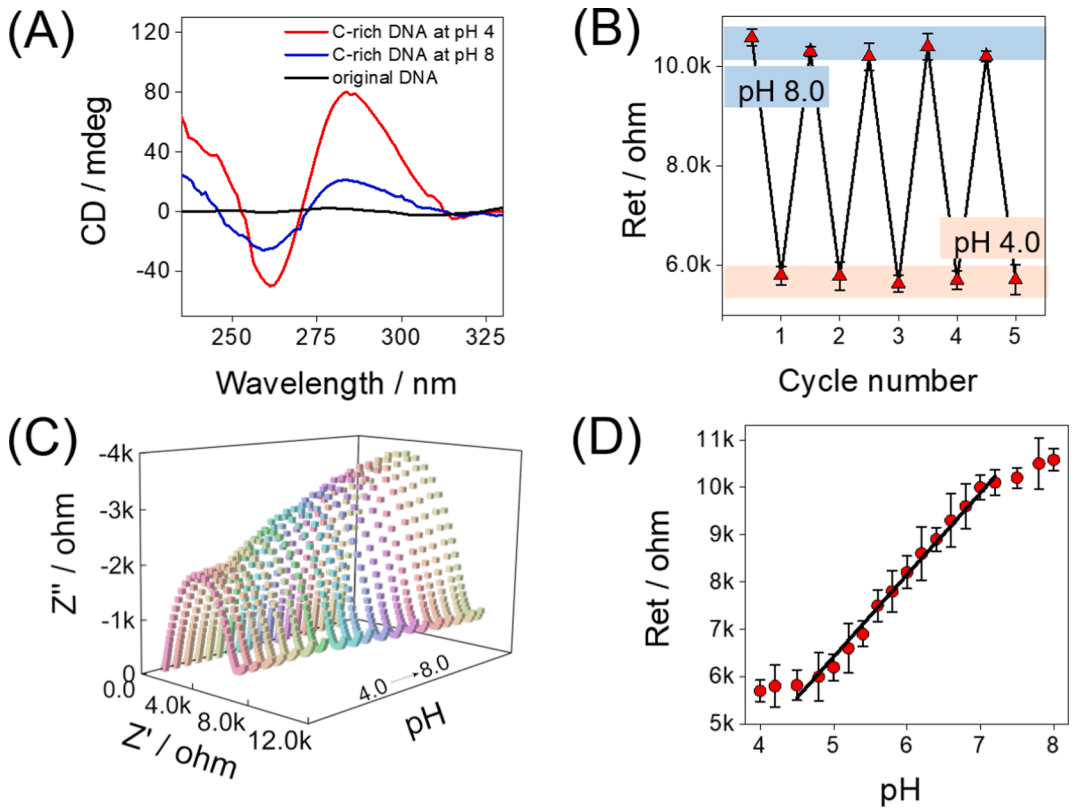

Fig. 2. Detection of pH: (A) CD spectra of original DNA, C-rich DNA in PB (100 mM, pH 4.0) and PB (100 mM, pH 8.0); (B) EIS reversibility of the proposed biosensor in PB (100 mM, pH 4.0) and PB (100 mM, pH 8.0) alternately; (C) EIS responses of the prepared biosensor after incubating in PB with different pHs (4.0, 4.2, 4.5, 4.8, 5.0, 5.2, 5.4, 5.6, 5.8, 6.0, 6.2, 6.4, 6.6, 6.8, 7.0, 7.2, 7.5, 7.8, and 8.0); (D) The linear relationship of the proposed pH sensor between EIS response value (Ret) and pH value.

3.1. Principle of the assay

Previous studies have demonstrated that the intercalated motif (i-motif) structure is a four-stranded DNA secondary structure, which is formed by stacking intercalated cytosine-protonated cytosine ($C:C^+$) pairs [1-3]. Also, TdT can catalyze the addition of multiple deoxynucleotide triphosphates (dNTPs) to the free 3′–OH terminus of single-stranded DNA [26-28], and the density and distribution of dNTP determine the sequence and length of TdT-yielded DNAs. Inspired by these two cases, an enough long C-rich DNA, which is extended by TdT polymeric interaction, can associate in the weak acid condition to form abundant intramolecular C-style tetraplexes (namely i-motifs), and this can be ascribed to that a fraction of the C bases can be protonated in a slightly acidic environment [1-3]. Scheme 1 illustrates the fabrication process and application of the cascade i-motifs-dependent reversible electrochemical impedance biosensor. Firstly, the 5′-thiol-terminated original DNA is assembled on Au electrode surface via Au-S bonds. In the presence of TdT, the 3′-OH end of original DNA is initiated by the continuous addition of dCTP to form a long C-rich DNA. What is noteworthy is that the TdT-yielded C-rich DNAs can lead to an obvious EIS response because of the strong repulsion to the $[Fe(CN)_6]^{3-/4-}$ probe; on the contrary, C bases can be partially protonated under acidic conditions, and the protonated C^+ and the unprotonated C can form many i-motifs in this system by means of hydrogen bonding pairs, resulting in a significant decrease in the EIS response. Meanwhile, subtle changes in pH also are an index of many diseases, since it reveals that there are some major changes in metabolism, thus giving rise to certain diseases. Based on it, our proposed cascade i-motifs-dependent biosensor can be applied well for investigating two factors including pH and TdT in complex microenvironment.

The formation of C-rich DNA is a key factor of the designed cascade i-motifs system, so gel electrophoresis, dynamic light scattering, square wave voltammetry (SWV), and UV–vis spectra were employed for proving it. As expected, some clear and dispersive gel electrophoresis bands (lane 2) appear relative to original DNA (lane 1) (Fig. 1A). Meanwhile, a marked difference emerges for the size distribution (Fig. 1B), presenting an obvious increase after the treatment of TdT. These results give clearly a direct evidence for the extension of original DNA. Next, in view of the interaction of C-Ag(I)-C, we design an electrochemical method to verify the C-rich structure, and a SWV peak at + 0.15 V (anodic stripping peak) increases sharply (Fig. 1C), which is corresponding to electrochemical characteristic peak of Ag(I) [37]. Additionally, a frequently used method for AuNPs-based sensing, which takes advantage of the colloidal stability and color change, is employed to identify the role of TdT. Normally, adsorption of unfolded short DNA can increase the stability of the AuNPs against salt to retain the red color. Once a DNA become more longer, it's not easy to adsorb tightly the AuNPs surface or it is possible to form a folded intramolecular and intermolecular complex, then its adsorption by AuNPs is hindered, and the AuNPs are easily aggregated by salt to give a blue color. As illustrated in Fig. 1D, the extinction of AuNPs at 520 nm gets smaller after TdT extension, not only that we indeed observe the expected color change of the AuNPs from red to purple. All the outcomes above confirm the construction of TdT-yielded C-rich DNAs successfully.

3.2. The monitoring of pH

The i-motif has a characteristic CD spectrum with a dominant positive band at about 290 nm and a negative band at around 260 nm [3,38]. In our work, can TdT-yielded C-rich DNAs form this so-called i-motif structure? We record their CD spectra under pH 4.0 or pH 8.0. As shown in Fig. 2A, a characteristic positive and negative CD peak illustrated

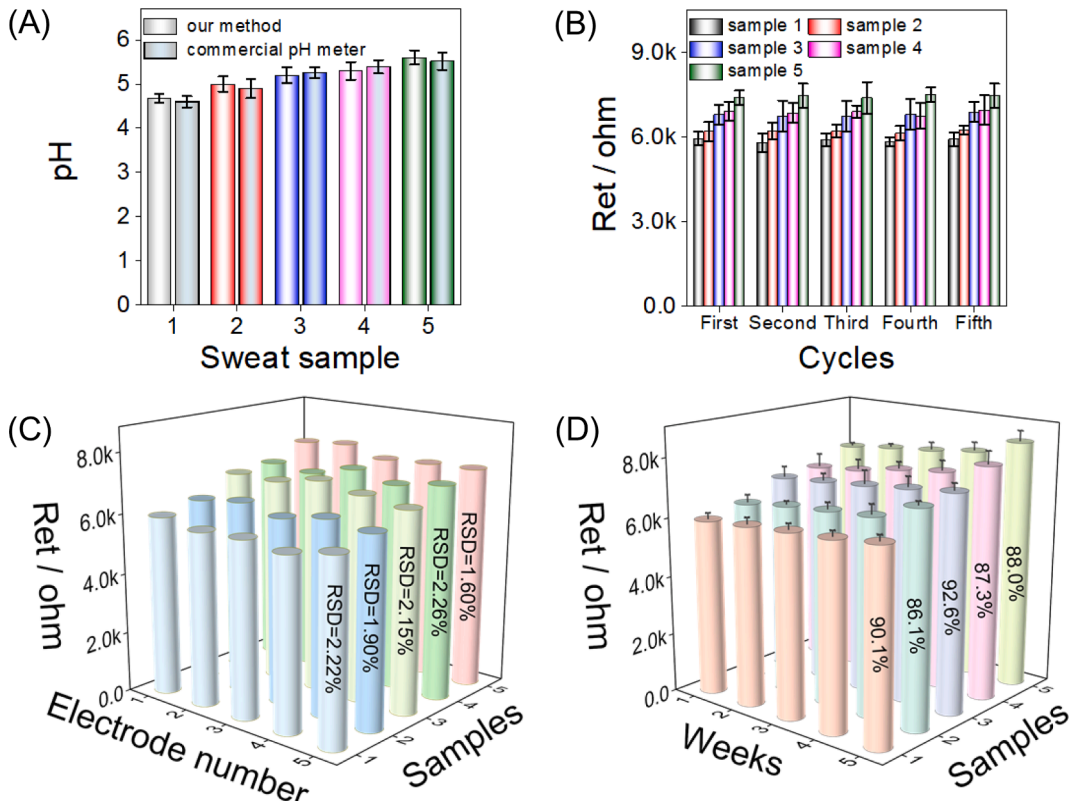

Fig. 3. Detection of pH in different sweat samples: (A) The comparison on pH between our method and commercial pH meter (1, 2, 3, 4, and 5, sort by pH value); (B) Repeatability for our proposed biosensor by determining the samples five times; (C) Reproducibility by using five different batches of biosensors; (D) Storage stability by testing the same biosensors every week, and put it in the refrigerator when not in use.

above for TdT-yielded C-rich DNA at pH 8.0 is observed in comparison to that of original DNA. Additionally, the positive peak at about 290 nm and the negative peak at approximately 260 nm become stronger at pH 4. The results suggest the TdT-yielded C-rich DNA can form the preferable i-motif structures at pH 4.0. Later, we attach original DNA and TdT-yielded C-rich DNA onto Au electrode surface to test their EIS responses. On the one hand, there is a sharp increase for EIS response due to the longer TdT-yielded C-rich DNA relative to original DNA (Fig. S1A), thus enhancing the repelling force to the $[Fe(CN)_6]^{3-/4-}$ probe; on the other hand, the EIS response deceases significantly as the pH goes down to 4 (Fig. S1B), and the greater electron transfer rate can be attributed to the positively charged i-motifs formed at slight acidic condition to draw electrostatically $[Fe(CN)_6]^{3-/4-}$ close to the Au electrode surface. Thus, whether this EIS change is dominated by the configuration change of i-motifs or the effect of pHs? So, we make a comparison of bare Au electrode and DNA-modified Au electrode at different PB containing 5 mM $[Fe(CN)_6]^{3-/4-}$. As expected, there is slightly potential difference and negligible current change for the cyclic voltammetry with a change in pH (Fig. S1C, 1D), and the EIS value stays about the same on even ground for bare Au electrode and original DNA modified electrode as the pH changes (Fig. S1E, 1F), illustrating that the system (EIS signal) is dominated by the configuration change of i-motifs, rather than the pH of the electrolyte solution.

Furthermore, we explore the reversible behavior of cascade i-motifs-dependent electrochemical impedance biosensor under pH 8.0 and 4.0 conditions alternately (Fig. 2B). More exciting is that EIS responses vary regularly, and some bigger EIS responses at pH 8.0 and some smaller EIS responses at pH 4.0 are found clearly, which is like an reversible EIS signal switch, indicating that the system can adapt to the changes in pH and presents a huge potential in pH monitoring.

After it, we incubate the prepared biosensor in a series of PB solutions with different pHs, and the EIS curves are shown in Fig. 2C. The EIS responses increase gradually with the increasing pHs (from 4.0 to 8.0), indicating that the i-motif structure of TdT-yielded C-rich DNA could form in acidic solution because of semi-protonation and keep a single-stranded DNA state in weakly basic or basic solution. As depicted in Fig. 2D, the curve of EIS response *versus* pH shows a wide dynamic response range from pH 4.0 to 8.0. In the beginning, there is a slower increase in the range of 4 to 4.5. Next, the EIS response increases radically with the pH in the range of 4.5 to 7.2 owing to the rapid structural transition between single-stranded DNA and i-motif structures, and a good linear relationship is observed in this range with a sensitivity of 1751 O/pH (Ret = 1751pH − 2365) and the correlation coefficient is 0.990. When the pH exceeds 7.2, the changes are smaller again because there are no i-motifs basically under slightly alkaline conditions. After it, we compare our cascade i-motifs-dependent electrochemical impedance strategy with other methods (Table S1), and a wider dynamic response range (pH 4 to 8) and a better linear response (pH 4.5 to 7.2) are exhibited fully, which are suitable perfectly for investigating the relationship between pH and clinical pathological in human skin or cell. Moreover, we employ the C30 modified electrode as control to verify this phenomenon (Fig. S2). As expected, there is basically no change at the bare electrode and original DNA modified electrode before and after pH change; whereas the other two electrodes show a similar alteration in EIS signal along with the change of pH, but the more significant change occurs at TdT-mediated electrode due to the formation of long C-rich DNAs, illustrating further the feasibility and advantages of our method.

As is well-known, the pH of a healthy and hydrated skin is in the range of 4.2 to 5.6 [39,40], so the pH of the sweat discharged from the body is also slightly acidic, approximately from 4.5 to 5.5, nevertheless it can also be influenced by other extra factors. We make use of our proposed method to test the pH of sweat samples taken from different human bodies, and the results are compared to that tested by commercial miniature pH meter (Fig. 3A). Obviously, there is no significant

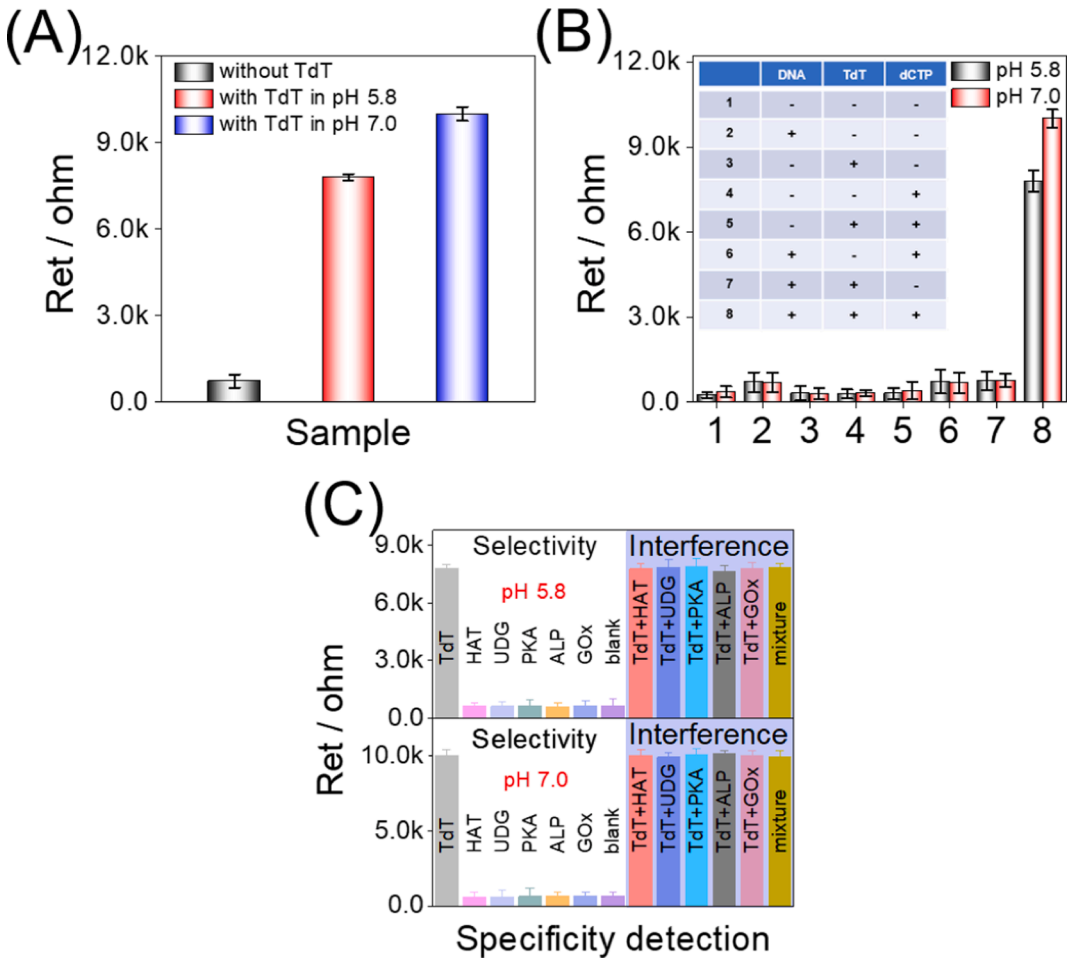

Fig. 4. Detection of TdT activity: (A) EIS responses in the absence or presence of TdT and (B) investigating the role of component solution for TdT analysis, inset: the detailed composition of solution; (C) Specificity and interference of the prepared biosensor under different pHs states.

difference in these comparisons, indicating our method used in the pH test is feasible and the analytical result is effective. Five parallel experiments directed at the five samples are employed for discussing the repeatability of our method (Fig. 3B), and the effective signal basically has no variation after 5 times testing, showing a very high repeatability to pH test. Next, the fabrication reproducibility is investigated by measuring the pH at five different samples. As expected, these electrodes prepared by the same process exhibit similar signal response and the relative standard deviations (RSDs) for pH test are from 1.60% to 2.26% (Fig. 3C). Furtherly, we evaluate the stability of the designed sensors stored in the refrigerator at 4 °C before use. As presented in Fig. 3D, the electrochemical EIS signal shows a slow downward trend, and keeps about 92.6% or 86.0% of its initial electrochemical signal after 3 weeks or 5 weeks, respectively. The good stability might be related to simple electrochemical modification layers (only DNA monolayer, no complex cyclic program). All the results above indicate that our prepared biosensor can effectively sense the changes in pH with good repeatability, excellent reproducibility, and acceptable stability.

3.3. *The sensing of TdT activity and its inhibitors*

Recent studies show the abnormal activity of TdT is associated with an unfavorable prognosis of some cancer patients [33], and it is no doubt that TdT can act as a biomarker for cancer; more importantly, the development of cancer is often accompanied by a certain degree of changes in pH in the human body. Hence, this biosensor above is of great scientific significance in abnormal TdT-induced cancer diseases. To acquire the best sensing performance, we first optimize various experimental conditions of the prepared biosensor before testing, such as the TdT-mediated extension time and temperature, the concentration of dCTP, and the incubation time in PB (100 mM, pH 5.8) and PB (100 mM, pH 7.0). As depicted in Fig. S3, an extension time of 180 min, a polymerization temperature of 37 °C, a concentration of 10 mM dCTP, and an incubation time in PB of 25 min are confirmed by a series of optimization experiments.

Under the optimized conditions, we further investigate the capacity of the biosensor to probe TdT activity in different pH conditions. Generally, intracellular pH is between 6.8 and 7.4 in the cytosol or between 5.0 and 6.0 in the cell's acidic organelles such as lysosome, so we choose the two pH values (5.8 or 7.0) as the discussion points. As shown in Fig. 4A, the R_{et} value increases significantly due to the formation of the long C-rich DNA under TdT catalytic polymerization, however, a higher R_{et} value appears at pH 7.0, and the trend is in keeping with the results of Fig. 2 above. This might be originated from the positively charged i-motifs formed at slight acidic condition to electrostatically attract redox pair $[Fe(CN)_6]^{3-/4-}$ close to the electrode surface. To illustrate the unique phenomenon, we also discuss the role of the key - factor in TdT catalytic reaction, and there is an effective EIS signal only when all the factors exist at the same time the system (Fig. 4B). Additionally, selectivity is also one of the decisive factors on whether the biosensor can be used for TdT analysis in the complex system. We challenge the system with TdT and other related catalytic enzymes (such as HAT, UDG, PKA, ALP, and GOx) (Fig. 4C). There is an obvious EIS response for TdT, but the signal of other related catalytic enzymes is similar with the blank signal (original DNA modified electrode). Meanwhile, if other enzymes are added to TdT-derived reaction system,

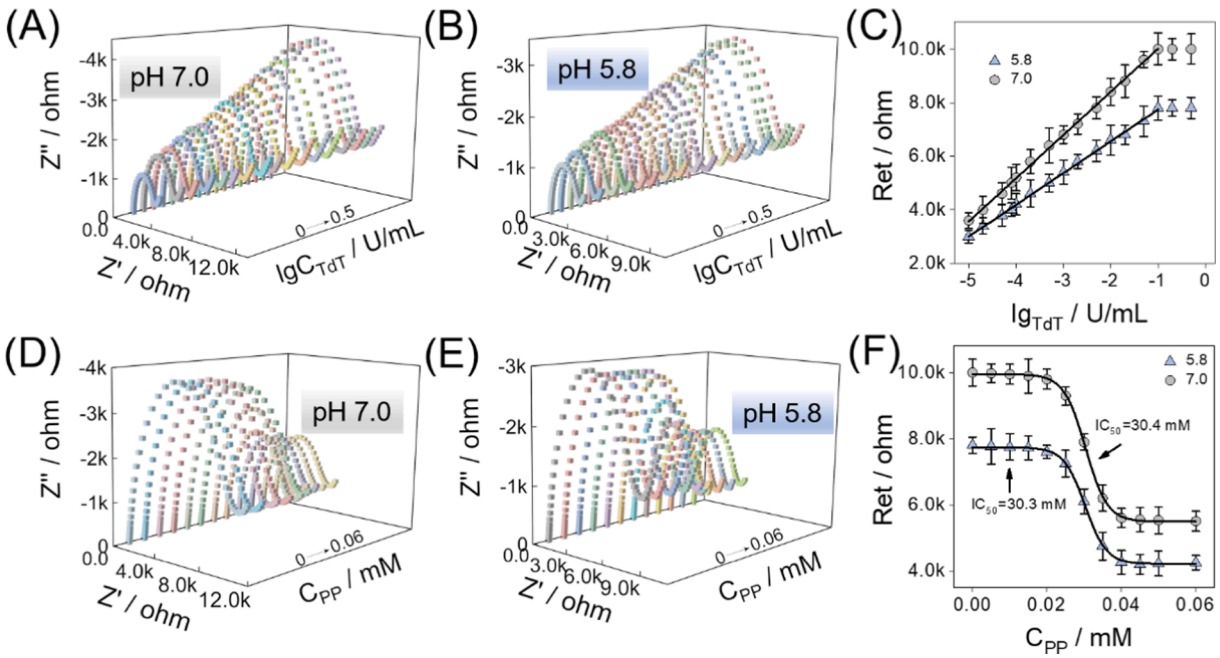

Fig. 5. TdT and its inhibitor analysis: EIS responses of the developed biosensors in PB (100 mM, pH 7.0 (A) or pH 5.8 (B)) toward TdT with different concentrations (0, 1×10^{-5}, 2×10^{-5}, 5×10^{-5}, 8×10^{-5}, 1×10^{-4}, 2×10^{-4}, 5×10^{-4}, 1×10^{-3}, 2×10^{-3}, 5×10^{-3}, 1×10^{-2}, 2×10^{-2}, 5×10^{-2}, 1×10^{-1}, 2×10^{-1}, and 5×10^{-1} U/mL); (C) The corresponding calibration curves plots by Ret *vs* the logarithm of TdT concentrations; The inhibition assay for TdT (0.1 U/mL) as a function of PP concentrations (0, 0.005, 0.01, 0.015, 0.02, 0.025, 0.03, 0.035, 0.04, 0.045, 0.05, and 0.06 mM) in PB (100 mM, pH 7.0) (D) or PB (100 mM, pH 5.8) (E) and (F) the corresponding calibration plots by Ret *vs* PP concentrations.

the EIS signal can also appear normally (no interference). These results suggest the biosensor possesses a good selectivity and anti-interference toward TdT detection.

Then, to meet the great needs of life sciences for TdT activity detection in complex environments, the EIS response upon different amounts of TdT is explored cautiously in different pH conditions. Because the growth of long C-rich DNA depends on TdT polymerization, the electrochemical signals gradually increase with increasing amounts of TdT at pH 7.0 (Fig. 5A). Interestingly, the same phenomenon can be observed at pH 5.8 (Fig. 5B), but it should be noted that the smaller EIS response under the same concentration appears at pH 5.8 relative to that at pH 7.0. In principle the transition from random coil to i-motif takes place in the pH range of 5.0–7.0, which can be tuned by the number of C bases [33,41]. In view of the above-mentioned facts, we suspect two reasons for the phenomenon: not all of C bases are protonated at pH 5.8; enough long C-rich DNA and limited electrode surface can lead to large steric hindrance. Fig. 5C presents two great linear correlations between EIS response and TdT amount in the range from 1×10^{-5} to 1×10^{-1} U/mL, hence, the most exciting thing is our sensor can be adapted to TdT analysis under different pH conditions. The linear relationships are given by Ret = 1612lgTdT + 11626, $R^2 = 0.9987$ (pH 7.0) and Ret = 1184lgTdT + 8922, $R^2 = 0.9984$ (pH 5.8), and the detection of limit is 0.79×10^{-5} U/mL (pH 7.0) and 0.25×10^{-5} U/mL (pH 5.8) (S/N = 3), respectively. As listed in Table S2, we compare the analytical performance of our method to some previous methods, and the minimum detection concentration is no worse than other methods. Therefore, this sensing method for tracing TdT analysis has great application potential in complex cell environment. Meanwhile, the screening of small molecule inhibitors for TdT activity is extremely important for drug discovery due to the maladjustment of TdT in some cancers. As shown in Fig. 5D and 5E, the introduction of $Na_4P_2O_7$ (PP) can result in an inhibition process in which EIS signal becomes progressively smaller, which is the opposite of the TdT test above, proving the feasibility of the prepared sensor in inhibitor screening. Then the IC_{50} value (half-maximum inhibitor concentration of the inhibitor) is 30.3 ± 2.5 μM (pH 5.8) or 30.4 ± 1.9 μM (pH 7.0) (Fig. 5F), respectively, which are similar to the literature value [34,35,42].

Next, when the biosensor is stored in the fridge (4 °C) for the fifth week, the EIS responses can retain 85.7% (pH 5.8) or 90.8% (pH 7.0) of its initial value, respectively (Fig. S4A). Moreover, the repeatability is also discussed by using the same biosensor for 5 parallel tests and the RSD of the EIS response is found to be 3.15% (pH 5.8) or 2.73% (pH 7.0), respectively, indicating an outstanding repeatability for our method (Fig. S4B). To assess the applicability and reliability of the designed sensor for clinical samples, we choose the lysates of common MCF-7 cell and Hela cell as study model. PB solution was used for regulating the pH of the cell lysates at 7.0 and 5.8, and the recovery experiments are carried out by using cell samples with different pHs. As can be seen from Table S3, the spike recoveries range from 90.0% to 105.0%, which is acceptable for quantitative assays performed in real samples. Thus, the detection strategy has good potential application for probing TdT in real samples.

4. Conclusions

An electrochemical EIS switch is developed on basis of the conformational changes of C-rich DNA probe produced by TdT's catalytic extension in different pHs. This novel switch is firstly constructed due to the following highlights: pH-dependent cascade i-motifs are created by TdT-mediated long C-rich DNAs; electrochemical EIS technology is employed for accomplishing pH and TdT analysis; the proposed biosensor with simple DNA interface is well-suited for monitoring the change of pH and the detection of TdT activity in real microenvironment. On the one hand, the change of pH can cause the comformational change of DNA from free state to i-motif; on the other hand, the amount of TdT can influence the EIS response tremendously, and this gives it the ability to probe TdT activity in complex matrix. The results indicate that the developed cascade i-motifs probe has outstanding analytical performance for pH and TdT detection such as simple modified layer, excellent sensitivity and selectivity, and remarkable practicability and reliability. This sheds new light on the importance of the deprotonated structures because the i-motif conformations can be

discussed as a new class of possible biological signals for cancers and other diseases, and the designed strategy has important scientific implications for pH- or TdT-related *in situ* clinical examination/diagnosis and drug discovery in the future.

Declaration of Competing Interest

The authors declare that they have no known competing financial interests or personal relationships that could have appeared to influence the work reported in this paper.

Acknowledgments

Financial support from the National Natural Science Foundation of China (42076193), the Ningbo Municipal Natural Science Foundation (202002N3178, and 202003N4185), Zhejiang Provincial Natural Science Foundation of China (LY20B050005), Scientific Research Project of Education Department of Zhejiang Province (Y202147697), and University-level Project of Ningbo College of Health Sciences (2019Y01) are gratefully acknowledged.

Appendix A. Supplementary data

Supplementary data to this article can be found online at https://doi.org/10.1016/j.bioelechem.2022.108085.

References

[1] P. Wolski, P. Wojton, K. Nieszporek, T. Panczyk, Interaction of human telomeric i-motif DNA with single-walled carbon nanotubes: insights from molecular dynamics simulations, J. Phys. Chem. B 123 (2019) 10343–10353.
[2] D. Zhao, H. Tang, H. Wang, C. Yang, Y. Li, Analytes triggered conformational switch of i-motif DNA inside gold-decorated solid-state nanopores, ACS Sens. 5 (7) (2020) 2177–2183.
[3] A. Lopez, B. Liu, Z. Huang, F. Zhang, J. Liu, Fluorescein-stabilized i-motif DNA and its unfolding leading to a stronger adsorption affinity, Langmuir 35 (36) (2019) 11932–11939.
[4] K. Gehring, J.-L. Leroy, M. Guéron, A tetrameric DNA structure with protonated cytosine-cytosine base pairs, Nature 363 (6429) (1993) 561–565.
[5] L. Shi, F. Cao, L. Zhang, Y. Tian, I-motif formed at physiological pH triggered by spatial confinement of nanochannels: an electrochemical platform for pH monitoring in brain microdialysates, Anal. Chem. 92 (2020) 4535–4540.
[6] J.C.G. Jeynes, K. Geraki, C. Jeynes, M.i. Zhaohong, A.A. Bettiol, E. Latorre, L. W. Harries, C. Soeller, Nanoscale properties of human telomeres measured with a dual purpose X-ray fluorescence and super resolution microscopy gold nanoparticle probe, ACS Nano 11 (12) (2017) 12632–12640.
[7] Y. Ding, A.M. Fleming, L. He, C.J. Burrows, Unfolding kinetics of the human telomere i-motif under a 10 pN force imposed by the α-hemolysin nanopore identify transient folded-state lifetimes at physiological pH, J. Am. Chem. Soc. 137 (28) (2015) 9053–9060.
[8] D. Miao, Y. Yu, Y. Chen, Y. Liu, G. Su, Facile construction of i-motif DNA-conjugated gold nanostars as near-infrared and pH dual-responsive targeted drug delivery systems for combined cancer therapy, Mol. Pharm. 17 (4) (2020) 1127–1138.
[9] G. Pan, Q. Mou, Y. Ma, F. Ding, J. Zhang, Y. Guo, X. Huang, Q. Li, X. Zhu, C. Zhang, pH-Responsive and gemcitabine-containing DNA nanogel to facilitate the chemodrug delivery, ACS Appl. Mater. Interfaces 11 (44) (2019) 41082–41090.
[10] Z. Zhou, D. Fan, I. Willner, Modeling gene expression instability by programmed and switchable polymerization/nicking DNA nanomachineries, ACS Nano 14 (4) (2020) 5046–5052.
[11] Z. Qing, J. Hu, J. Xu, Z. Zou, Y. Lei, T. Qing, R. Yang, An intramolecular catalytic hairpin assembly on a DNA tetrahedron for mRNA imaging in living cells: improving reaction kinetics and signal stability, Chem. Sci. 11 (2020) 1985–1990.
[12] P. Peng, Q. Wang, Y.i. Du, H. Wang, L. Shi, T. Li, Extracellular ion-responsive logic sensors utilizing DNA dimeric nanoassemblies on cell surface and application to boosting AS1411 internalization, Anal. Chem. 92 (13) (2020) 9273–9280.
[13] Z. Qing, J. Xu, J. Zheng, L. He, Z. Zou, S. Yang, W. Tan, R. Yang, In situ amplification-based imaging of RNA in living cells, Angew. Chem. Int. Edit. 58 (2019) 11574–11585.
[14] A. Nakamura, C. Oki, S. Sawada, T. Yoshii, K. Kuwata, A.K. Rudd, N.K. Devaraj, K. Noma, S. Tsukiji, Designer palmitoylation motif-based self-localizing ligand for sustained control of protein localization in living cells and caenorhabditis elegans, ACS Chem. Biol. 15 (4) (2020) 837–843.
[15] M.T. Ghoneim, A. Nguyen, N. Dereje, J. Huang, G.C. Moore, P.J. Murzynowski, C. Dagdeviren, Recent progress in electrochemical pH-sensing materials and configurations for biomedical applications, Chem. Rev. 119 (8) (2019) 5248–5297.
[16] J. Zhao, Y. Li, M. Yu, Z. Gu, L. Li, Y. Zhao, Time-resolved activation of pH sensing and imaging in vivo by a remotely controllable DNA nanomachine, Nano Lett. 20 (2) (2020) 874–880.
[17] L. Zhou, C. Cheng, X. Li, J. Ding, Q. Liu, B. Su, Nanochannel templated iridium oxide nanostructures for wide-range pH sensing from solutions to human skin surface, Anal. Chem. 92 (5) (2020) 3844–3851.
[18] L. Wang, Y.i. Xie, Y. Yang, H. Liang, L.i. Wang, Y. Song, Electroactive covalent organic frameworks/carbon nanotubes composites for electrochemical sensing, ACS Appl. Nano Mater. 3 (2) (2020) 1412–1419.
[19] D. Gu, W. Yang, G. Ning, F. Wang, S. Wu, X. Shi, Y. Wang, Q. Pan, In situ ligand formation-driven synthesis of a uranyl organic framework as a turn-on fluorescent pH sensor, Inorg. Chem. 59 (3) (2020) 1778–1784.
[20] F. Yu, X. Jing, W. Lin, Single-/dual-responsive pH fluorescent probes based on the hybridization of unconventional fluorescence and fluorophore for imaging lysosomal pH changes in Hela cells, Anal. Chem. 91 (23) (2019) 15213–15219.
[21] X. Zhao, S. Campbell, G.Q. Wallace, A. Claing, C.G. Bazuin, J.-F. Masson, Branched Au nanoparticles on nanofibers for surface-enhanced raman scattering sensing of intracellular pH and extracellular pH gradients, ACS Sens. 5 (7) (2020) 2155–2167.
[22] J.E. Park, N. Yonet-Tanyeri, E. Vander Ende, A.-I. Henry, B.E. Perez White, M. Mrksich, R.P. Van Duyne, Van Duyne, Plasmonic microneedle arrays for in situ sensing with surface-enhanced raman spectroscopy (SERS), Nano Lett. 19 (10) (2019) 6862–6868.
[23] C. Xu, F. Wu, P. Yu, L. Mao, In vivo electrochemical sensors for neurochemicals: recent update, ACS Sens. 4 (12) (2019) 3102–3118.
[24] C.J. Valentine, K. Takagishi, S. Umezu, R. Daly, M. De Volder, Paper-based electrochemical sensors using paper as a scaffold to create porous carbon nanotube electrodes, ACS Appl. Mater. Inter. 12 (27) (2020) 30680–30685.
[25] H. Chen, X. Pang, Z. Ni, M. Liu, Y. Zhang, S. Yao, Upconversion nanoparticles with bright red luminescence for highly sensitive quantifying alkaline phosphatase activity based on target-triggered fusing reaction, Anal. Chim. Acta 1095 (2020) 146–153.
[26] A. Fang, H. Chen, H. Li, M. Liu, Y. Zhang, S. Yao, Glutathione regulation-based dual-functional upconversion sensing-platform for acetylcholinesterase activity and cadmium ions, Biosens. Bioelectron. 87 (2017) 545–551.
[27] L.M. Chang, F.J. Bollum, Cyclic AMP-dependent phosphorylation of terminal deoxynucleotidyl transferase, J. Biol. Chem. 257 (16) (1982) 9588–9592.
[28] S. Barthel, S. Palluk, N.J. Hillson, J.D. Keasling, D.H. Arlow, Enhancing terminal deoxynucleotidyl transferase activity on substrates with 3′ terminal structures for enzymatic De Novo DNA synthesis, Genes 11 (2020) 102.
[29] K. Kidoguchi, M. Yokoo, A. Umino, S. Aoki, S. Kimura, Terminal deoxynucleotidyl transferase (TdT) negative early T cell precursor acute lymphoblastic leukemia (ETP-ALL) with spontaneous acute kidney injury, Ann. Hematol. 99 (4) (2020) 885–886.
[30] R. Costi, G. Cuzzucoli Crucitti, L. Pescatori, A. Messore, L. Scipione, S. Tortorella, A. Amoroso, E. Crespan, P. Campiglia, B. Maresca, A. Porta, I. Granata, E. Novellino, J. Gouge, M. Delarue, G. Maga, R. Di Santo, New nucleotide-competitive non-nucleoside inhibitors of terminal deoxynucleotidyl transferase: discovery, characterization, and crystal structure in complex with the target, J. Med. Chem. 56 (2013) 7431–7441.
[31] L.-J. Wang, M.-L. Luo, Q. Zhang, B.o. Tang, C.-Y. Zhang, Single quantum dot-based nanosensor for rapid and sensitive detection of terminal deoxynucleotidyl transferase, Chem. Commun. 53 (80) (2017) 11016–11019.
[32] W. Tian, G. Wang, X. Liu, W. Ren, C. Liu, Z. Li, A terminal extension-actuated isothermal exponential amplification strategy toward the ultrasensitive and versatile detection of enzyme activity in a single cell, Talanta 211 (2020) 120704.
[33] X. Liu, H. Wang, K. Deng, S. Kwee, H. Huang, L. Tang, Single primer based multisite strand displacement reaction amplification strategy for rapid detection of terminal deoxynucleotidyl transferase activity, Anal. Chem. 91 (11) (2019) 7482–7486.
[34] D. Hu, Y. Hu, Q. Zhang, P. Ran, X. Liu, Y. Zheng, Z. Guo, S. Wang, D.i. Wu, Label-free electrochemical strategy for probing TdT and Exo I activity by silver-based square wave voltammetry, J. Electrochem. Soc. 166 (12) (2019) B1028–B1033.
[35] Y. Hu, Q. Zhang, Z. Guo, S. Wang, C. Du, C. Zhai, In situ grown DNA nanotail-templated silver nanoclusters enabling label-free electrochemical sensing of terminal deoxynucleotidyl transferase activity, Biosens. Bioelectron. 98 (2017) 91–99.
[36] Y. Hu, Q. Shen, W. Li, Z. Liu, Z. Nie, S. Yao, A TdT-mediated cascade signal amplification strategy based on dendritic DNA matrix for label-free multifunctional electrochemical biosensing, Biosens. Bioelectron. 63 (2015) 331–338.
[37] X. Jin, L. Zhou, B.o. Zhu, X. Jiang, N. Zhu, Silver-dendrimer nanocomposites as oligonucleotide labels for electrochemical stripping detection of DNA hybridization, Biosens. Bioelectron. 107 (2018) 237–243.
[38] Z. Huang, B. Liu, J. Liu, Parallel polyadenine fuplex formation at low pH facilitates DNA conjugation onto gold nanoparticles, Langmuir 32 (2016) 11986–11992.
[39] I.H. Blank, Measurement of pH of the skin surface, J. Invest. Dermatol. 2 (1939) 67–74.
[40] G.K. Mani, Y. Nimura, K. Tsuchiya, Advanced artificial electronic skin based pH sensing system for heatstroke detection, ACS Sens. 5 (4) (2020) 911–916.
[41] J. Mergny, L. Lacroix, X. Han, J. Leroy, C. Helene, Masthead, J. Am. Chem. Soc. 117 (1995) 8887–8898.
[42] Q.Q. Zhang, D.D. Hu, T.Y. Zhan, Y.F. Hu, Z.Y. Guo, S. Wang, Tailored DNA nano-framework-enabled Medusa electrochemiluminescence immunosensor for quantitative detection of histone acetyltransferase, Sens. Actuators B: Chem. 316 (2020) 128165.